Coupled thermo-hydro-mechanical double structure model for expansive soils

D. Mašín

Charles University in Prague

Faculty of Science

Albertov 6

12843 Prague 2, Czech Republic

E-mail: masin@natur.cuni.cz

Tel: +420-2-2195 1552, Fax: +420-2-2195 1556

ABSTRACT

In this paper, development of a thermo-hydro-mechanical model for expansive soils including double structure is described. The model is based on the previously developed double structure hypoplastic model, in which the hydro-mechanical coupling is considered at each of the two structural levels. The model also includes separate effective stress definitions and water retention curves for the two levels of structure and they are linked through the double-structure coupling function. In the proposed model, thermal effects are considered both on the mechanical behaviour of macrostructure and microstructure. This is combined with a temperature-dependent water retention curve for the macrostructure and an enhanced double-structure coupling law. Good predictions of the model are

demonstrated by comparing the simulations with experimental data on MX80 bentonites taken from the literature.

Keywords: Expansive soils, Bentonite, Hypoplasticity, Double structure, Thermo-hydro-mechanical coupling

INTRODUCTION

Thermo-hydro-mechanical modelling of the behaviour of expansive clays is important in a number of high-priority applications, such as the design of nuclear waste repositories. Their behaviour is, however, remarkably complex, in particular due to their double-structure nature. Each of the structural levels respond differently to temperature change, suction change and mechanical action. In this paper, an advanced model is developed aiming to predict these complex phenomena in a unified manner.

The model presented is an advance with respect to the double structure hydro-mechanical hypoplastic model proposed by Mašín (2013b). The structure of this paper is as follows. This earlier double structure model is described first. Subsequently, literature review on the thermal behaviour of both macrostructure and microstructure is presented, based on which an enhanced model is developed. Due to the complex nature of the model and for the sake of conciseness of the paper, only those features which are new with respect to the original model are discussed in detail, while complete model formulation is presented in Appendix. Predictions of the proposed model are compared with experimental data on compacted MX80 bentonite taken from the literature.

Notation and conventions: Compact tensorial notation is used throughout. Second-order tensors are denoted with bold letters (e.g. $\boldsymbol{\sigma}$, $\mathbf{N}$) and fourth-order tensors with cal-

ligraphic bold letters (e.g. $\boldsymbol{\mathcal{L}}$, $\boldsymbol{\mathcal{A}}$). Symbols "$\cdot$" and ":" between tensors of various orders denote inner product with single and double contraction, respectively. The dyadic product of two tensors is indicated by "$\otimes$", and $\|\dot{\boldsymbol{\epsilon}}\|$ represents the Euclidean norm of $\dot{\boldsymbol{\epsilon}}$. The trace operator is defined as $\mathrm{tr}\,\dot{\boldsymbol{\epsilon}} = \mathbf{1} : \dot{\boldsymbol{\epsilon}}$; $\mathbf{1}$ and $\boldsymbol{\mathcal{I}}$ denote second-order and fourth-order unity tensors, respectively. Following the sign convention of continuum mechanics, compression is taken as negative. However, Roscoe's variables $p = -\mathrm{tr}\,\boldsymbol{\sigma}/3$ and $\epsilon_v = -\mathrm{tr}\,\boldsymbol{\epsilon}$, and pore fluid and gas pressures u_w and u_a are defined to be positive in compression. The operator $\langle x \rangle$ denotes the positive part of any scalar function x, thus $\langle x \rangle = (x + |x|)/2$. The effective stress is denoted as $\boldsymbol{\sigma}$, net stress $\boldsymbol{\sigma}^{net} = \boldsymbol{\sigma}^{tot} + \mathbf{1}u_a$, where $\boldsymbol{\sigma}^{tot}$ is total stress. Matric suction is defined as $s = u_a - u_w$. Macrostructural quantities are identified by superscript ^{M}, microstructural quantities by superscript ^{m}.

EXISTING HYDRO-MECHANICAL DOUBLE STRUCTURE MODEL

The model described in this paper has been developed using double-structure framework, originally proposed by Alonso et al. (1999). The model is based on the hydro-mechanical double structure hypoplastic model by Mašín (2013b). This model is briefly described in this section.

The hypoplastic double structure model, and the double structure models in general, are based on the assumption supported by various micro-mechanical studies that in expansive soils one can identify two levels of structure: A so-called macrostructure, which is representing an assembly of silt-size aggregates of the clay particles, and a so-called microstructure, which is representing the internal structure of these aggregates. A conceptual sketch of these two levels of structure is in Fig. 1.

In the model by Mašín (2013b), separate models are considered for the mechanical and

hydraulic responses of microstructure and macrostructure. These responses are coupled at each structural level, and additionally, the behaviour of the two structural levels is linked through the double-structure coupling function. Schematic representation of the adopted modelling approach is shown in a sketch in Fig. 2. The individual models are denoted as G^M, G^m, H^M and H^m respectively.

In the particular double structure model from Mašín (2013b), the mechanical behaviour of macrostructure (G^M) was described using the model for unsaturated soils by Mašín and Khalili (2008), which itself was based on hypoplastic model for saturated clays from Mašín (2005). Hydraulic response of macrostructure (H^M) was based on the void-ratio dependent water retention model from Mašín (2010). Microstructure has always been considered as fully saturated (simple H^m model). Its mechanical behaviour (G^m) was reversible volumetric, governed by the Terzaghi effective stress principle: see Mašín and Khalili (2016) for thorough discussion on this subject. The $G^M H^M$ coupling was accomplished by the dependency of H^M on volume change, and by the dependency of the effective stress on degree of saturation of macrostructure S_r^M. The $G^m H^m$ coupling was introduced through the adoption of the Terzaghi effective stress for the mechanical behaviour of microstructure. Finally, the double structure coupling was controlled by a function of relative void ratio, which evolved from the original proposition by Alonso et al. (1999).

The general rate formulation of the double structure hypoplastic model reads

$$\mathring{\boldsymbol{\sigma}}^M = f_s \left[\boldsymbol{\mathcal{L}} : (\dot{\boldsymbol{\epsilon}} - f_m \dot{\boldsymbol{\epsilon}}^m) + f_d \mathbf{N} \| \dot{\boldsymbol{\epsilon}} - f_m \dot{\boldsymbol{\epsilon}}^m \| \right] + f_u \mathbf{H}_s \tag{1}$$

where $\mathring{\boldsymbol{\sigma}}^M$ is the objective effective stress rate of macrostructure, $\dot{\boldsymbol{\epsilon}}$ is the global Euler stretching tensor, $\dot{\boldsymbol{\epsilon}}^m$ represents the microstructural strain rate, $\boldsymbol{\mathcal{L}}$, $\mathbf{N}$ are fourth- and

second- order hypoplastic tensors, f_d, f_s and f_u are hypoplastic scalar factors (see Mašín (2013a) and Mašín and Khalili (2008) for more details), f_m is the double-structure coupling factor and $\mathbf{H}_s$ is the factor enabling wetting-induced collapse predictions.

Central to the model were definitions of macro- and microstructural state variables. The following variables were adopted: S_r^M (degree of saturation of macrostructure), defined as water volume in macropores over total macropore volume, S_r^m (degree of saturation of microstructure), defined as water volume in micropores over total micropore volume, e^M (macrostructural void ratio), defined as ratio of macropore volume over total volume of *aggregates* and e^m (microstructural void ratio), defined as ratio of micropore volume over volume of solids. Note that the definitions of S_r^M and e^M are different than assumed in previous double-structure models, which had certain advantages for the model formulation. Their definition implied the following relationships between microstructural, macrostructural and global quantities:

$$\dot{\boldsymbol{\epsilon}} = \dot{\boldsymbol{\epsilon}}^M + f_m \dot{\boldsymbol{\epsilon}}^m \tag{2}$$

$$S_r = S_r^M + \frac{e^m}{e}(S_r^m - S_r^M) \tag{3}$$

$$e = e^M + e^m + e^M e^m \tag{4}$$

$$\frac{\dot{e}}{1+e} = \operatorname{tr} \dot{\boldsymbol{\epsilon}} \tag{5}$$

$$\frac{\dot{e}^M}{1+e^M} = \operatorname{tr}\left[\dot{\boldsymbol{\epsilon}}^M + (f_m - 1)\dot{\boldsymbol{\epsilon}}^m\right] \tag{6}$$

$$\frac{\dot{e}^m}{1+e^m} = \operatorname{tr} \dot{\boldsymbol{\epsilon}}^m \tag{7}$$

In addition to the macro- and microstructural state variables, crucial for the model performance is the definition of the stress measures adopted in the model formulation.

The effective stress of macrostructure ($\boldsymbol{\sigma}^M$) has been defined as (Alonso et al. 2010)

$$\boldsymbol{\sigma}^M = \boldsymbol{\sigma}^{net} - \mathbf{1} S_r^M s \tag{8}$$

where $\boldsymbol{\sigma}^{net}$ is the net stress and s is matric suction. The macrostructural effective stress depends on S_r^M, which depends on suction and on macrostructural void ratio. This dependency must be taken into account when evaluating rate form of Eq. (8):

$$\mathring{\boldsymbol{\sigma}}^M = \mathring{\boldsymbol{\sigma}}^{net} - \mathbf{1}\left[\frac{\partial(S_r^M s)}{\partial s}\dot{s} + \frac{\partial(S_r^M s)}{\partial e^M}\dot{e}^M\right] \tag{9}$$

Following Mašín and Khalili (2016), the microstructural effective stress is defined simply as

$$\boldsymbol{\sigma}^m = \boldsymbol{\sigma}^{net} - \mathbf{1} s \tag{10}$$

An important quantity in Eqs. (2) - (7) is the double structure coupling factor f_m. It has the following properties. When $f_m = 1$, pure swelling or shrinking of aggregates implies the same global swelling or shrinking of the soil. Contrary, $f_m = 0$ means that the aggregates freely penetrate or recede from the macropores while inducing no global sample deformation. As explained in detail in Mašín (2013b), the actual deformation mode depends on the level of compaction of macrostructure, which is measured by void ratio e. Minimum void ratio e_d corresponds to $e^M = 0$, i.e. $e_d = e^m$ (note that e^m varies with stress level, so also e_d is a variable). Maximum void ratio e_i corresponds to the state at the

isotropic normal compression line. It is then convenient to define relative void ratio r_{em} as

$$r_{em} = \frac{e - e_d}{e_i - e_d} \tag{11}$$

For the densest possible state $r_{em} = 0$ and for the loosest possible state $r_{em} = 1$.

For aggregate swelling (wetting or unloading process) $f_m \rightarrow 1$ corresponds to a dense macrostructure (no macropore occlusion), whereas $f_m \rightarrow 0$ corresponds to a loose macrostructure (full occlusion of macropores by swelling aggregates). The following relationship, satisfying these limiting properties has been adopted in Mašín (2013b) for $\dot{p}^m < 0$:

$$f_m = 1 - (r_{em})^m \tag{12}$$

where m is model parameter controlling the influence of r_{em} on f_m for intermediate values of r_{em}. For particle shrinkage ($\dot{p}^m > 0$), $f_m = 0$ has always been assumed. The parameter m controls the influence of macrostructure compaction on the double structure coupling.

THE INFLUENCE OF TEMPERATURE ON THE BEHAVIOUR OF MACROSTRUCTURE AND MICROSTRUCTURE

Temperature affects the behaviour of expansive soils through various effects, which will briefly be discussed in this section. We will consider separately its effect on the individual models, that is G^M, G^m, H^M and H^m respectively.

As for the mechanical behaviour of macrostructure, temperature influences position of the normal compression lines (NCL) of a soil. A majority of experimental data show that in the applied stress range the NCLs at different temperatures may be considered parallel to each other (an exception to this trend can be found in (Romero et al. 2003; Tanaka

et al. 1997), while with increasing temperature the specific volume at the NCL for the given effective mean stress p^M decreases. Most of the data available are on non-expansive soils (Uchaipchat and Khalili 2009; Campanella and Mitchell 1968; Cekerevac and Laloui 2004; Burghignoli et al. 2000). Similar results have, however, been reported on bentonites (Tang et al. 2008). It should be noted that the normal compression line represents the maximum void ratio the soil can be at the given mean stress and temperature, therefore heating-induced shift of the NCL position implies heating-induced soil compaction of loosely compacted soils. It has been reported both for non-expansive soils (Del Olmo et al. 1996; Hueckel and Baldi 1990; Baldi et al. 1988; Sultan et al. 2002; Demars and Charles 1982), and on bentonites (Tang et al. 2008). These effects are considered in the proposed constitutive model by assuming that the asymptotic state boundary surface depends on temperature, as is described in more detail in Section 4.

Temperature also affects mechanical response of microstructure. It influences both the basal spacing and thus the amount of crystalline water and also the diffuse double layer thickness. The influence of temperature on hydration state of Na- and Ca- montmorillonite has been studied by Morodome and Kawamura (2009). In Na-montmorillonites, they observed that *for the given hydration state* the basal spacing is not affected by temperature significantly. However, with increasing temperature the clay stacks tend to stay longer in the lower hydration state during wetting, which means that increasing temperature decreased stack volume. Contrary, more gradual decrease of basal spacing with temperature was observed in Ca-montmorillonites. Different effect of temperature from that on basal spacing is observed on the diffuse double layer thickness. As discussed by Yong et al. (1963), diffuse double layer theory (Gouy 1910; Chapman 1913; Mitchell and Soga 2005)

and also its more advanced alterantives (Yong and Mohamed 1992; Komine and Ogata 1999; Sridharan and Choudhury 2002; Tripathy et al. 2004), predicts an increase of double layer thickness with temperature. At the same time, however, increasing temperature causes a decrease of dielectric constant, which in turn implies a decrease of double layer thickness with temperature. These contradictory effects cause the effect of temperature on microstructure not to be unique and they have to be studied individually for specific soil and pore-water chemistry. Experimental results support this finding. In some clays, contraction and decrease of swelling pressures was reported with temperature, for example in FEBEX bentonite (Romero et al. 2005; Villar and Lloret 2004). In other clays, expansion and increase of swelling pressures was reported with temperature, like in MX80 bentonite (Tang et al. 2008)). It also appears that the contradicting effects can in some cases cancel-out, leading to swelling pressures more-or-less independent of temperature, as reported by Zhang et al. (1993). Due to the above reasons, constitutive model for swelling clays should be general and should allow for both swelling and contraction of microstructure with temperature, controlled by a parameter.

In the water retention behaviour, it is difficult to distinguish experimentally the response of macrostructure and microstructure. The data on non-expansive single-structure soils indicate that increasing temperature decreases the air-entry value of suction (Uchaipchat and Khalili 2009) and thus the water retention capacity. In general, this could be caused by a change of surface tension of water with temperature, however, different researchers (Romero et al. 2001; Villar and Lloret 2004; Jacinto et al. 2009) observed more significant decrease of water retention capacity than would be implied by the change of surface tension only. It is to be pointed out that the global water retention capacity is influenced by

both the water retention capacity of macrostructure and of microstructure. As microstructure may be considered as saturated up to large values of suction (Martin 1960; Gens and Alonso 1992; Alonso et al. 1999; Yong 1999; Fityus and Buzzi 2009), temperature-induced microstructural swelling would also imply increase of water retention capacity, and microstructural shrinkage would imply decrease of water retention capacity. The global water retention capacity then reflects interplay between the above mentioned effects. Most experimental studies (Villar and Lloret 2004; Yong et al. 1963; Jacinto et al. 2009) indicate slight decrease of the global water retention capacity with temperature. A simplified approach is chosen in the present work, in which the effect of temperature on water retention capacity of macrostructure is considered to depend solely on the change of surface tension of water with temperature without considering the effect of variable grain-water interface contact angle. The global water retention capacity is then implied by both the retention of macrostructure and specific volume of (saturated) microstructure, which are linked through the double structure coupling framework.

PROPOSED THERMO-HYDRO-MECHANICAL MODEL

Model formulation

In the proposed model, thermal effects on the behaviour of macrostructure and microstructure have been incorporated. Complete formulation of the new model is described in Appendix A. In this section, new features with respect to the hydro-mechanical model from Mašín (2013b) are described.

The complete model takes the following rate form:

$$\mathring{\boldsymbol{\sigma}}^{M} = f_s \left[\boldsymbol{\mathcal{L}} : (\dot{\boldsymbol{\epsilon}} - f_m \dot{\boldsymbol{\epsilon}}^m) + f_d \mathbf{N} \| \dot{\boldsymbol{\epsilon}} - f_m \dot{\boldsymbol{\epsilon}}^m \| \right] + f_u \left(\mathbf{H}_s + \mathbf{H}_T \right) \tag{13}$$

where $\boldsymbol{\mathcal{L}}$, $\mathbf{N}$, $\mathbf{H}_s$ and $\mathbf{H}_T$ are hypoplastic tensors, f_s, f_d and f_u are hypoplastic scalar factors, $\dot{\boldsymbol{\epsilon}}$ is the Euler stretching tensor, $\mathring{\boldsymbol{\sigma}}^M$ is the objective effective stress rate of macrostructure and $\dot{\boldsymbol{\epsilon}}^m$ is microstructural strain rate.

When compared with the model from Mašín (2013b), a new mechanical hypoplastic model for saturated soils by Mašín (2013a) is adopted as a base mechanical model for macrostructure. The model incorporates explicit formulation of the asymptotic state boundary surface. The model has also been extended to incorporate stiffness anisotropy effects (Mašín 2014). While stiffness anisotropy is not crucial for the performance of the model regarding expansive soils predictions, the possibility to prescribe anisotropic response of macrostructure has been retained in the new model. This modification required re-evaluation of the hypoplastic tensors $\boldsymbol{\mathcal{L}}$ and $\mathbf{N}$ from Eq. (13) and associated quantities, refer to Eqs. (44) - (73) in Appendix A.

The thermal behaviour of macrostructure is described by an approach developed by Mašín and Khalili (2012). The model assumes temperature-dependent normal compression lines of the form:

$$\ln(1+e) = N(s,T) - \lambda^*(s,T) \ln \frac{p^M}{p_r} \tag{14}$$

where p^M is the effective mean stress of macrostructure, p_r is the reference stress of 1 kPa, s is suction and T is temperature (measured in Kelvin). $N(s,T)$ and $\lambda^*(s,T)$ are temperature- and suction-dependent positions and slopes of normal compression lines,

respectively. They are defined as

$$N(s,T) = N + n_s \left\langle \ln \frac{s}{s_e} \right\rangle + n_T \ln\left(\frac{T}{T_r}\right) \qquad \lambda^*(s,T) = \lambda^* + l_s \left\langle \ln \frac{s}{s_e} \right\rangle + l_T \ln\left(\frac{T}{T_r}\right) \tag{15}$$

where N, n_s, n_T, l_s, l_T are parameters, T_r is a reference temperature and s_e is water retention model variable. Note that in most cases the slope of normal compression line is independent of temperature and thus $l_T = 0$.

A modification has to be included in the formulation of the model to ensure consistency with the prescribed normal compression line: as discussed in Wong and Mašín (2014), the model would predict gradual drift from the normal compression line in mechanical loading, if the slope $\lambda^*(s,T)$ would be used in formulation of $\boldsymbol{\mathcal{L}}$ and $\mathbf{N}$. The reason is as follows: loading changes macrostructural void ratio, which affects the value of s_e, which, in turn, affects $N(s,T)$ and $\lambda^*(s,T)$ through Eq. (15). Therefore, even during mechanical loading at constant suction, the value $N(s,T)$ and $\lambda^*(s,T)$ vary and the actual (tangent) value of the compression index is different than the compression index calculated from $\lambda^*(s,T)$. To remedy this problem, the model components must be expressed in terms of the actual (tangent) value of λ^*, denoted as λ^*_{act}. Derivation of λ^*_{act} for the proposed model is explained in Appendix B, the final expression reads:

$$\lambda^*_{act} = \frac{\lambda^*(s,T) e^M \left(1+e^m\right) - \kappa_m \left(1+e^m\right) \left(p^M/p^m\right) \left[(1+e^M)(n_s - l_s \ln(p^M/p_r)) + f_m e^M\right]}{e^M(1+e^m) - (1+e)(n_s - l_s \ln(p^M/p_r))} \tag{16}$$

For consistency with the prescribed normal compression lines, tensor $\mathbf{H}_T$ (heating-induced compaction factor) had to be included into the model formulation (13) in addition

to the tensor $\mathbf{H}_s$ (wetting-induced compaction factor). General equation for $\mathbf{H}_T$ reads (Mašín and Khalili 2012)

$$\mathbf{H}_T = \frac{c_i \boldsymbol{\sigma}^M}{p_e} \frac{\partial p_e}{\partial T} \dot{T} \tag{17}$$

where the additional factor c_i has been introduced in Mašín and Khalili (2012). Evaluation of $\partial p_e / \partial T$ using (15) leads to the following expression for $\mathbf{H}_T$:

$$\mathbf{H}_T = \frac{c_i \boldsymbol{\sigma}^M}{T \lambda^*_{act}} \left(n_T - l_T \ln \frac{p_e}{p_r} \right) \langle \dot{T} \rangle \tag{18}$$

Unlike in the single-structure hypoplastic model, the factors $\mathbf{H}_s$ and $\mathbf{H}_T$ do not fully guarantee consistency of the state with the state boundary surface during its shrinkage (wetting and heating). The reason is as follows: Eq. for $\mathbf{H}_s$ is based on the expression for $\dot{p}_e$ (equation (76) in Appendix A), which is assumed to depend on suction only. However, in the coupled model, it depens also on e^M and on temperature through their additional effect on s_e (because s_e is involved in Eq. (15)). As it is not possible to express model equations analytically in this complex case, another approach has been followed. The factor f_u from (13) has been expressed as

$$f_u = \begin{cases} \left(\frac{p^M}{p^{MA}} \right)^m & \text{for} \quad p^M \leq p^{MA} \\ \left(\frac{p^M}{p^{MA}} \right)^{100} & \text{for} \quad p^M > p^{MA} \end{cases} \tag{19}$$

where p^{MA} is the value of macrostructural effective stress corresponding to the current stress ratio at the asymptotic state boundary surface. p^{MA} may be calculated as $p^{MA} = p_e (f_d^A)^{1/\alpha_f} / 2$. Principle of the expression (19) is as follows. For (inallowed) out-of-state boundary surface states with $p^{MA} < p^M$, the value of f_u quickly reaches very high values,

which ensures that the state does not drift-away from the state boundary surface even though $\mathbf{H}_s$ and $\mathbf{H}_T$ do not guarantee it with analytical accuracy.

The water retention model for macrostructure is based on the hysteretic model from Mašín (2013b). The air-entry value of suction s_{en} is, however, considered to be temperature-dependent. It is controlled by an equation

$$s_{en} = s_{e0} \frac{e_0^M}{e^M} \left(\frac{a + bT}{a + bT_r} \right) \tag{20}$$

The model requires three reference values, namely the reference air-entry value of suction s_{e0} for the reference macrostructural void ratio e_0^M and reference temperature T_r. In addition, the thermal part of the model requires two parameters a and b. As pointed out by Grant and Salehzadeh (1996), their values a=0.18 N/m and b=-0.00015 N/(mK) imply that the effects of temperature by water retention capacity are caused solely by its effect on surface tension without an effect of temperature on grain-water interface contact angle and other effects. This has not been supported by experimental observations (Romero et al. 2001; Villar and Lloret 2004; Jacinto et al. 2009). She and Sleep (1998) concluded that the experimental data do not agree with the model even if the effect of grain-water interface contact angle is taken into account. It is to be pointed out, however, that the cited experimental observations evaluated global water contents, which are in the present model affected also by microstructural void ratio.

Microstructure is considered to be fully saturated. Following the work by Mašín and Khalili (2016), its mechanical response is considered to be governed by the Terzaghi effective stress principle with additional strains induced by temperature variation. The thermal

deformation is considered to be fully reversible, governed by the coefficient α_s using

$$\dot{\boldsymbol{\epsilon}}^{mT} = \frac{\mathbf{1}}{3}\alpha_s \dot{T} \tag{21}$$

where $\dot{\boldsymbol{\epsilon}}^{mT}$ is the thermal strain rate of the microstructure and $\mathbf{1}$ is the second-order identity tensor. Therefore, depending on the value of α_s it is possible to prescribe both microstructural swelling and contraction with temperature. In combination with the suction- and mechanical action-induced deformation, the complete expression for $\dot{\boldsymbol{\epsilon}}^{m}$ reads:

$$\dot{\boldsymbol{\epsilon}}^{m}_{nom} = \frac{\mathbf{1}}{3}\left(\alpha_s \dot{T} - \frac{\kappa_m}{p^m}\dot{p}^m\right) \tag{22}$$

$$\dot{\boldsymbol{\epsilon}}^{m} = (1 - f_{ul})\dot{\boldsymbol{\epsilon}}^{m}_{nom} \tag{23}$$

with parameter κ_m. The factor f_{ul} has the following reason within the model. In highly swelling clays, it is possible that under certain circumstances swelling of the aggregates is higher than the global bulk modulus implied by the slope of the normal compression line. Then, the state could in swelling surpass normal compression line, which is unphysical on one hand and implies bad convergence of the model on the other. The factor f_{ul} reduces swelling for states close to the asymptotic state boundary surface. The expression for f_{ul} is similar, but not identical, to f_u (Eq. (19)). It reads

$$f_{ul} = \begin{cases} \left(\frac{p^M}{p^{MA}}\right)^m & \text{for} \quad p^M \leq p^{MA} \quad \text{and} \quad \dot{\boldsymbol{\epsilon}}^{m}_{nom} > 0 \\ 1 & \text{for} \quad p^M > p^{MA} \quad \text{and} \quad \dot{\boldsymbol{\epsilon}}^{m}_{nom} > 0 \\ 0 & \text{for} \quad \dot{\boldsymbol{\epsilon}}^{m}_{nom} \leq 0 \end{cases} \tag{24}$$

therefore, f_{ul} never exceeds 1 and it is zero for microstructural compression, where its contribution is not needed.

Microstructural void ratio e^m can be initialised through:

$$e^m = \exp\left[\kappa_m \ln \frac{s_r}{p^m} + \ln(1 + e^m_{r0}) + \alpha_s \left(T - T_r\right)\right] - 1 \tag{25}$$

where p^m is the microstructural effective mean stress and κ_m is a parameter. e^m_{r0} represents reference void ratio of microstructure for the reference temperature T_r, reference suction s_r and zero total stress. Due to the factor f_{ul}, Eq. (25) is not an analytical integration of (22) and the microstructural response is not fully reversible.

In the original model, the double structure coupling function f_m has been assumed as zero for aggregate shrinkage. In the present model calibrated to MX80 data, however, this assumption leads to underprediction of global shrinkage in cooling experiments. The experimental data (Fig. 5) indicate that the global shrinkage in cooling depends on suction. The following equation has been proposed for particle shrinkage which was found to lead to good representation of experiments:

$$f_m = c_{sh}\left(\frac{s}{s_e}\right) \tag{26}$$

where c_{sh} is a parameter. f_m is bound within the range 0 to 1. The complete formulation for f_m then reads

$$f_m = \begin{cases} 1 - (r_{em})^m & \text{for} \quad \dot{p}^m \leq 0 \\ \left\langle \frac{c_{sh} s}{s_e} \right\rangle & \text{for} \quad \dot{p}^m > 0 \end{cases} \tag{27}$$

$f_m = 1$ if Eq. (27) leads to $f_m > 1$. r_{em} is relative void ratio quantified in Appedix A.

The above equations imply the objective rate of the macrostructural effective stress $\mathring{\boldsymbol{\sigma}}^M$. General expression, including thermal effects, reads

$$\mathring{\boldsymbol{\sigma}}^M = \mathring{\boldsymbol{\sigma}}^{net} - \mathbf{1}\left[\frac{\partial(S_r^M s)}{\partial s}\dot{s} + \frac{\partial(S_r^M s)}{\partial e^M}\dot{e}^M + \frac{\partial(S_r^M s)}{\partial T}\dot{T}\right] \tag{28}$$

Substituting partial derivatives into (28) leads to

$$\mathring{\boldsymbol{\sigma}}^M = \mathring{\boldsymbol{\sigma}}^{net} - \mathbf{1}S_r^M\left[(1-\gamma r_\lambda)\dot{s} - \gamma s\frac{\dot{e}^M}{e^M} + \frac{\gamma s b\dot{T}}{a+bT}\right] \tag{29}$$

Finally, physical meaning of all the model parameters is briefly summarised in Table 1.

The following experiments are ideally needed for calibration of all the model parameters:

1. Triaxial tests on saturated samples for calibration of φ_c and ν.
2. Suction- and temperature- controlled oedometric or triaxial isotropic loading tests (at different constant values of temperature and suction) for calibration of λ^*, N, n_s, l_s, n_T, l_T.
3. Wetting and/or heating test of slightly overconsolidated soil for calibration of m.
4. Heating or cooling test at highly compacted samples for calibration of α_s.
5. Unloading tests at highly compacted samples for calibration of κ_m (a default value of κ^*, for example $\kappa^* = 0.01$, can be assumed for calibration).

Solution of $\mathring{\boldsymbol{\sigma}}^M$ for the general THM loading

Eq. (13) is not straightforward to solve for loading input obtained from the finite element code with known $\dot{\boldsymbol{\epsilon}}$, $\dot{s}$ and $\dot{T}$, because total stress rate appears both in the formulation of $\dot{\boldsymbol{\epsilon}}^m$ and in the formulation of $\mathring{\boldsymbol{\sigma}}^M$, thus on both the right- and left-hand side of Eq. (13). A numerical procedure has been used to solve this equation, which has been implemented into an in-house general purpose thermo-hydro-mechanical single element code (Janda and Mašín 2016). The algorithm is described below:

$TOL = \text{round\_to\_digits}(\|\dot{\boldsymbol{\epsilon}}\|/1000)$;
if $(TOL < 1.e-10)$ then $TOL = 1.e-10$;
$i = 1$;
$\text{tr}\,\dot{\boldsymbol{\epsilon}}_{iter}^{m(i)} = 0$;
$err^{(i)} = 1$;
calculate $\boldsymbol{\mathcal{L}}$, f_d, f_u;
while $err^{(i)} > TOL$ **do**
  calculate $f_m^{(i)}$;
  calculate $\lambda_{act}^{*(i)}$;
  calculate $\mathbf{N}^{(i)}$, $\mathbf{H}_T^{(i)}$, $\mathbf{H}_s^{(i)}$, $f_s^{(i)}$;
  $\dot{\boldsymbol{\epsilon}}_{iter}^{m(i)} = \frac{\mathbf{1}}{3}\,\text{tr}(\dot{\boldsymbol{\epsilon}}_{iter}^{m(i)})$;
  $\dot{\boldsymbol{\epsilon}}^{M(i)} = \dot{\boldsymbol{\epsilon}} - f_m^{(i)}\dot{\boldsymbol{\epsilon}}_{iter}^{m(i)}$;
  $\dot{e}^{M(i)} = (1+e^M)\,\text{tr}\left[\dot{\boldsymbol{\epsilon}}^{M(i)} + (f_m^{(i)}-1)\dot{\boldsymbol{\epsilon}}_{iter}^{m(i)}\right]$;
  $\mathring{\boldsymbol{\sigma}}^{net(i)} = f_s^{(i)}\left(\boldsymbol{\mathcal{L}} : \dot{\boldsymbol{\epsilon}}^{M(i)} + f_d\mathbf{N}^{(i)}\|\dot{\boldsymbol{\epsilon}}^{M(i)}\|\right) + f_u\left(\mathbf{H}_s^{(i)} + \mathbf{H}_T^{(i)}\right) +;$
    $\mathbf{1}S_r^M\left[(1-\gamma r_\lambda)\dot{s} - \gamma s\frac{\dot{e}^{M(i)}}{e^M} + \frac{\gamma s b\dot{T}}{a+bT}\right]$;
  $\dot{p}^{m(i)} = \frac{1}{3}\,\text{tr}\,\mathring{\boldsymbol{\sigma}}^{net(i)} - \dot{s}$;
  $\text{tr}\,\dot{\boldsymbol{\epsilon}}^{m(i)} = f_{ul}\left(\alpha_s\dot{T} - \frac{\kappa_m}{p^m}\dot{p}^{m(i)}\right)$;
  $err^{(i)} = |\,\text{tr}\,\dot{\boldsymbol{\epsilon}}^{m(i)} - \text{tr}\,\dot{\boldsymbol{\epsilon}}_{iter}^{m(i)}|$;
  $\text{tr}\,\dot{\boldsymbol{\epsilon}}_{iter}^{m(i+1)} = (\text{tr}\,\dot{\boldsymbol{\epsilon}}^{m(i)} + 3\,\text{tr}\,\dot{\boldsymbol{\epsilon}}_{iter}^{m(i)})/4$;
  $i = i+1$;
end

MODEL EVALUATION

Description of the material and experiments

The model has been evaluated with respect to experimental data on compacted bentonite by Tang and Cui (2007) and Tang et al. (2008). They studied the behaviour of MX80 bentonite from Wyoming, USA, under non-isothermal conditions. Two experimental data sets have been adopted.

The first one has been published by Tang and Cui (2007). They studied water retention behaviour of a compacted bentonite in suction- and temperature-controlled isotropic cell. Prior to the test, the samples had the initial suction slightly lower than 145 MPa (140 MPa was assumed in the simulations) and the initial dry density was 16.5 kN/m^3. Subsequently, different values of total suction were applied using vapour equilibrium technique and water content of samples was measured until it has stabilised.

The second experimental data set has been published by Tang et al. (2008). The samples have been tested in suction- and temperature-controlled isotropic cell capable of application of high suctions using vapour equilibrium technique, high temperatures (up to 80 °C) and high mechanical isotropic stresses (up to 60 MPa). Prior to testing, compacted specimens with an initial suction of 110 MPa and dry densities of approx. 17.5 kN/m^3 were machined to obtain the required dimensions (80 mm in diameter, 10-15 mm in height). Thereafter, suction was changed using vapour equilibrium technique to the desired values (9, 39 and 110 MPa in three experimental sets) while measuring the swelling deformation. Samples were then placed into the cell and loaded to the initial isotropic total stress of 0.1 MPa. This was the initial state for subsequent thermo-mechanical testing. For the detailed description of the tests the reader is referred to Tang et al. (2008).

Description of the modelling procedure

In the simulations, complete thermo-hydro-mechanical histories of the samples have been followed. That is, the initial state for the given thermo-hydro-mechanical experimental stage has not been prescribed, but it has instead been simulated from the common initial state. All the water retention curve simulations were performed from the initial state of total suction $s_t = 140$ MPa, $e = 0.64$, $T = 25°$C, $a_{scan} = 1$ and zero total stress. The initial stage has been followed by a change of temperature to the desired value and subsequent suction variation under zero total stress. The initial void ratio was calculated from the initial dry densities using specific gravity of grains $G_s = 2.76$ (Tang et al. 2008; Tang and Cui 2007).

The samples tested in the suction- and temperature-controlled isotropic cell had all have the initial state of $s_t = 110$ MPa, $e = 0.53$, $T = 25°$C, $a_{scan} = 0$ and zero total stress. The initial stage has been followed by a change of suction (in some cases), increase of total stress to 0.1 MPa and increase of temperature. Subsequent simulations followed the prescribed thermo-mechanical paths of each experiment.

Calibration of the model

Due to the limited number of experiments, the model has been calibrated using the data to be predicted. The experimental programme did not allow calibration of all the parameters. The additional parameters have been assumed, in particular taking into account calibration of the earlier versions of the model. It is to be pointed out that the assumed parameters do not affect substantially the model predictions.

Parameters of the basic hypoplastic model λ^* and κ^* have been calibrated using isotropic compression experiments (Fig. 7). Parameters N, n_s, n_T, l_s, l_T and m were adjusted so

the model properly predicted position of isotropic normal compression lines (Fig. 7) and also the heating-induced collapse/swelling strains (Fig. 5). Parameters φ_c and ν have been assumed.

Reference values s_r, e_0^M and T_r have been selected so they were within the range relevant for the present simulations (note that these values can be selected arbitrarily: if combined with appropriate value of e_{r0}^m they do not affect predictions). The corresponding e_{r0}^m has been adjusted for water retention curve predictions. The parameter κ_m controls both the swelling due to suction decrease (thermo-mechanical tests, Fig. 4) and water retention curves (Fig. 3) through its effect on e^m. The value of κ_m has thus been selected to predict accurately the swelling tests. It was observed that this value leads to overprediction of water content in water retention experiments at low suctions. Note that as very large strains (up to 50%) have been reached in swelling tests, the experimental data from (Tang et al. 2008) have been replotted in terms of natural strain for consistency with the modelling output (Fig. 4).

The value of α_s is controlling the thermal-induced swelling and it has been calibrated using heating tests at the suction of 110 MPa (Fig. 5). The parameters controlling water retention curve of macrostructure have little influence on results at very high suctions, s_{e0} and a_e have thus been assumed and a and b have selected considering that the effects of temperature on water retention capacity are caused solely by its effect on surface tension.

The set of parameters adopted in all the simulations is given in Table 2.

Model predictions

Model predictions are shown in Figures 3 to 7.

The predicted water retention curves are in Fig. 3. The dependency of water content

on suction is predicted correctly. The experiments show slight decrease of water retention capacity with temperature, the model predicts this dependency in a minor way only.

Figure 4 shows swelling due to wetting at zero total stress and constant temperature 25°C as measured on samples which have later been placed into the suction- and temperature-controlled isotropic cell. Swelling is slightly underpredicted, which is a consequence of optimization of the model calibration so that the parameters of the water retention curve are also predicted reasonably. Recall that complete thermo-hydro-mechanical histories of the samples have been simulated, the state reached after the wetting stage thus represents the initial state for subsequent simulations.

Volume strains due to heating at various values of suction and mean total stress are shown in Figure 5. The model is accurately predicting the observed complex behaviour. In particular:

- At high suctions (110 MPa), the model is correctly predicting swelling, whose magnitude is controlled by the parameter α_s. The heating-induced swelling at high suctions is primarily reversible (Fig. 5b).
- At lower values of suction (9 MPa for total stress of 0.1 MPa and 39 MPa for total stress of 5 MPa), the model is predicting heating-induced compaction ("collapse"). This compaction is irreversible and it is controlled by the offset of normal compression lines at different temperatures (by the parameters l_T and n_T). Still, for stress 0.1 MPa at suction 39 MPa the state is well within the state boundary surface and heating-induced swelling is predicted in agreement with experimental data. Note that, in principle, the model can also be calibrated using negative value of α_s to predict heating-induced contraction observed by some authors (Towhata

et al. 1993).

- Upon cooling, the model is predicting cooling-induced contraction. This contraction depends on suction, such that it is most pronounced at high suction of 110 MPa and least significant at lower values of suction (39 MPa and 9 MPa). These predictions are governed by the dependency of the double-structure coupling factor f_m on macrostructural degree of saturation (Eq. (26)).

For demonstration of the model response, Fig. 6 has been included which shows selected experiments from Fig. 5 with continued heating-cooling cycling (20 cycles in total). The cyclic accumulation is present due to the non-linear part of them model being active even at overconsolidated states. The model predicts cyclic accumulation of compaction for normally overconsolidated soil and cyclic accumulation of expansion of overconsolidated soil, which is in agreement with experimental data from literature (Di Donna and Laloui 2015).

The isotropic compression at various values of suction and temperature is shown in Fig. 7. The model predicts reasonably the initial void ratio, implied by wetting-induced swelling during the preceding experimental stage. Considering the effect of temperature, the model predicts lower position of the isotropic normal compression lines at higher temperatures (the parameter n_t has negative value). The difference appears to be insignificant in Fig. 7, but it is important for heating-induced compaction predictions shown in Fig. 5. Figure 7 shows that also the shape of the isotropic compression lines and the effect of suction on apparent preconsolidation pressure is predicted properly. Interesting insight into the model is in Fig. 7(c), where the isotropic compression curves are plotted in terms of macrostructural effective stress (recall that in the model the isotropic normal compression

lines are defined in terms of macrostructural effective stress). It is clear that the samples at $s = 9$ MPa swelled practically to the isotropic normal compression line, the curved shape of the isotropic curve in Fig. 7(b) is only due to transformation between net stress and macrostructural effective stress. Soil at $s = 39$ MPa and $s = 110$ MPa is in slightly overconsolidated state at the beginning of the isotropic compression.

CONCLUSIONS

A new thermo-hydro-mechanical model for expansive soils based on double structure concept and hypoplasticity has been developed. In the paper, the most important properties of the model have been presented. It has been shown that the model provides correct predictions of the complex behaviour of MX80 bentonite under various thermo-hydro-mechanical paths. In particular, the model properly predicts swelling or shrinkage in heating-cooling tests, depending on the current suction, total stress and void ratio. Also, global swelling of the samples due to wetting and the influence of suction and temperature on the shape and position of isotropic compression curves are well predicted. For the present calibration on MX80 bentonite, the model slightly overpredicts the global water content at low values of suction.

ACKNOWLEDGMENT

This work has been funded by the research grant 15-05935S of the Czech Science Foundation.

References

Alonso, E. E., Pereira, J.-M., Vaunat, J., and Olivella, S. (2010). "A microstructurally based effective stress for unsaturated soils." *Géotechnique*, 60(12), 913–925.

Alonso, E. E., Vaunat, J., and Gens, A. (1999). "Modelling the mechanical behaviour of expansive clays." *Engineering Geology*, 54, 173–183.

Baldi, G., Hueckel, T., and Pellegrini, R. (1988). "Thermal volume changes of the mineral - water system in low-porosity clay soils." *Canadian Geotechnical Journal*, 25, 807–825.

Burghignoli, A., Desideri, A., and Miliziano, S. (2000). "A laboratory study on the thermo-mechanical behaviour of clayey soils." *Canadian Geotechnical Journal*, 37, 764–780.

Campanella, R. G. and Mitchell, J. K. (1968). "Influence of temperature variations on soil behaviour." *Journal of the Soil Mechanics and Foundations Division ASCE*, 94(3), 709–734.

Cekerevac, C. and Laloui, L. (2004). "Experimental study of thermal effects on the mechanical behaviour of a clay." *International Journal for Numerical and Analytical Methods in Geomechanics*, 28, 209–228.

Chapman, D. L. (1913). "A contribution to the theory of electrocapillarity." *Phil. Mag.*, 25, 475–481.

Del Olmo, C., Fioravante, V., Gera, F., Hueckel, T., Mayor, J. C., and Pellegrini, R. (1996). "Thermomechanical properties of deep argillaceous formations." *Engineering Geology*, 41, 87–101.

Demars, K. R. and Charles, R. D. (1982). "Soil volume changes induced by temperature cycling." *Canadian Geotechnical Journal*, 19, 188–194.

Di Donna, A. and Laloui, L. (2015). "Response of soil subjected to thermal cyclic loading: Experimental and constitutive study." *Engineering Geology*, 190, 65–76.

Fityus, S. and Buzzi, O. (2009). "The place of expansive clays in the framework of unsat-

urated soil mechanics." *Applied Clay Science*, 43(2), 150–155.

Gens, A. and Alonso, E. (1992). "A framework for the behaviour of unsaturated expansive clays." *Canadian Geotechnical Journal*, 29, 1013–1032.

Gouy, G. (1910). "Sur la constitution de la charge à la surface d'un électrolyte." *J. Phys.*, 9, 457–468.

Grant, S. A. and Salehzadeh, A. (1996). "Calculation of temperature effects on wetting coefficients of porous solids and their capillary pressure functions." *Water Resources Research*, 32(2), 261–270.

Hueckel, T. and Baldi, G. (1990). "Thermoplasticity of saturated clays: Experimental constitutive study." *Journal of Geotechnical Engineering ASCE*, 116(12), 1778–1796.

Jacinto, A. C., Villar, M. V., Gómez-Espina, R., and Ledesma, A. (2009). "Adaptation of the van Genuchten expression to the effects of temperature and density for compacted bentonites." *Applied Clay Science*, 42, 575–582.

Janda, T. and Mašín, D. (2016). "General method for simulating laboratory tests with constitutive models for geomechanics." *(submitted)*.

Komine, H. and Ogata, N. (1999). "Prediction method for swelling characteristics of bentonite for nuclear waste disposal." *Proc. of the 7^{th} International Conference on Radioactive Waste Management and Environmental Remediation (CD-ROM)*.

Martin, R. T. (1960). "Adsorbed water on clay: a review." *Clays and Clay Minerals*, 9(1), 28–70.

Mašín, D. (2005). "A hypoplastic constitutive model for clays." *International Journal for Numerical and Analytical Methods in Geomechanics*, 29(4), 311–336.

Mašín, D. (2010). "Predicting the dependency of a degree of saturation on void ratio and

suction using effective stress principle for unsaturated soils." *International Journal for Numerical and Analytical Methods in Geomechanics*, 34, 73–90.

Mašín, D. (2013a). "Clay hypoplasticity with explicitly defined asymptotic states." *Acta Geotechnica*, 8(5), 481–496.

Mašín, D. (2013b). "Double structure hydromechanical coupling formalism and a model for unsaturated expansive clays." *Engineering Geology*, 165, 73–88.

Mašín, D. (2014). "Clay hypoplasticity model including stiffness anisotropy." *Géotechnique*, 64(3), 232–238.

Mašín, D. and Khalili, N. (2008). "A hypoplastic model for mechanical response of unsaturated soils." *International Journal for Numerical and Analytical Methods in Geomechanics*, 32(15), 1903–1926.

Mašín, D. and Khalili, N. (2012). "A thermo-mechanical model for variably saturated soils based on hypoplasticity." *International Journal for Numerical and Analytical Methods in Geomechanics*, 36(12), 1461–1485.

Mašín, D. and Khalili, N. (2016). "Swelling phenomena and effective stress in compacted expansive clays." *Canadian Geotechnical Journal*, 53(1), 134–147.

Mitchell, J. K. and Soga, K. (2005). *Fundamentals of soil behaviour, 3rd Edition*. John Wiley & Sons, Inc., Hoboken, New Jersey.

Morodome, S. and Kawamura, K. (2009). "Swelling behaviour of Na- and Ca- montmorillonite up to 150°C by *in situ* X-ray diffraction experiments." *Clays and Clay Minerals*, 57(2), 150–160.

Romero, E., Gens, A., and Lloret, A. (2001). "Temperature effects on the hydraulic behaviour of an unsaturated clay." *Geotechnical and Geological Engineering*, 19, 311–

332.

Romero, E., Gens, A., and Lloret, A. (2003). “Suction effects on a compacted clay under non-isothermal conditions.” *Géotechnique*, 53(1), 65–81.

Romero, E., Villar, N. V., and Lloret, A. (2005). “Thermo-hydro-mechanical behaviour of two heavily overconsolidated clays.” *Engineering Geology*, 81, 255–268.

She, H. Y. and Sleep, B. E. (1998). “The effect of temperature on capillary pressure-saturation relationships for air-water and perchlorethylene-water systems.” *Water Resources Research*, 34(10), 2587–2597.

Sridharan, A. and Choudhury, D. (2002). “Swelling pressure of sodium montmorillonites.” *Géotechnique*, 52(6), 459–462.

Sultan, N., Delage, P., and Cui, Y. J. (2002). “Temperature effects on the volume change behaviour of Boom clay.” *Engineering Geology*, 64, 135–145.

Tanaka, N., Graham, J., and Crilly, T. (1997). “Stress-strain behaviour of reconstituted illitic clay at different temperatures.” *Engineering Geology*, 47, 339–350.

Tang, A.-M. and Cui, Y.-J. (2007). “Controlling suction by vapour equilibrium technique at different temperatures, application to the determination of the water retention properties of MX80 clay.” *Canadian Geotechnical Journal*, 42, 287–296.

Tang, A.-M., Cui, Y.-J., and Barnel, N. (2008). “Thermo-mechanical behaviour of a compacted swelling clay.” *Géotechnique*, 58(1), 45–54.

Towhata, I., Kuntiwattanakul, P., Seko, I., and Ohishi, K. (1993). “Volume change of clays induced by heating as observed in consolidation tests.” *Soils and Foundations*, 33(4), 170–183.

Tripathy, S., Sridharan, A., and Schanz, T. (2004). “Swelling pressures of compacted ben-

tonites from diffuse double layer theory." *Canadian Geotechnical Journal*, 41, 437–450.

Uchaipchat, A. and Khalili, N. (2009). "Experimental investigation of thermo-hydro-mechanical behaviour of an unsaturated silt." *Géotechnique*, 59(4), 339–353.

Villar, M. V. and Lloret, A. (2004). "Influence of temperature on the hydro-mechanical behaviour of a compacted bentonite." *Applied Clay Science*, 26, 337–350.

Wong, K. S. and Mašín, D. (2014). "Coupled hydro-mechanical hypoplastic model for partially saturated soils incorporating small strain stiffness." *Computers and Geotechnics*, 61, 355–369.

Yong, R., Taylor, L. O., and Warkentin, B. P. (1963). "Swelling pressures of sodium montmorillonite at depressed temperature." *Proc. of the* 11^{th} *Nat. Conf. on Clays and Clay Minerals*, 268–281.

Yong, R. N. (1999). "Soil suction and soil-water potentials in swellig clays in engineered clay barriers." *Engineering Geology*, 54, 3–13.

Yong, R. N. and Mohamed, A. M. O. (1992). "A study of particle interaction energies in wetting of unsaturated expansive clays." *Canadian Geotechnical Journal*, 29, 1060–1070.

Zhang, F., Zhang, Z. Z., Low, P. F., and Roth, C. B. (1993). "The effect of temperature on the swelling of montmorillonite." *Clay Minerals*, 28, 25–31.

APPENDIX A - MODEL FORMULATION

The mathematical formulation of the proposed model for expansive soils is summarised in the following. The behaviour of two structural levels is linked through

$$\dot{\boldsymbol{\epsilon}} = \dot{\boldsymbol{\epsilon}}^M + f_m \dot{\boldsymbol{\epsilon}}^m \tag{30}$$

with the following void ratio measures and their relationships:

$$\frac{\dot{e}}{1+e} = \operatorname{tr} \dot{\boldsymbol{\epsilon}} \qquad \frac{\dot{e}^M}{1+e^M} = \operatorname{tr}\left[\dot{\boldsymbol{\epsilon}}^M + (f_m - 1)\dot{\boldsymbol{\epsilon}}^m\right] \qquad \frac{\dot{e}^m}{1+e^m} = \operatorname{tr} \dot{\boldsymbol{\epsilon}}^m \tag{31}$$

$$e = e^M + e^m + e^M e^m \tag{32}$$

$$S_r = S_r^M + \frac{e^m}{e}(S_r^m - S_r^M) \tag{33}$$

The mechanical behaviour of macrostructure is governed by

$$\mathring{\boldsymbol{\sigma}}^M = f_s\left(\boldsymbol{\mathcal{L}} : \dot{\boldsymbol{\epsilon}}^M + f_d \mathbf{N}\|\dot{\boldsymbol{\epsilon}}^M\|\right) + f_u\left(\mathbf{H}_s + \mathbf{H}_T\right) \tag{34}$$

$\boldsymbol{\sigma}^M$ is the macrostructural effective stress defined by

$$\boldsymbol{\sigma}^M = \boldsymbol{\sigma}^{net} - \chi^M s\mathbf{1} \tag{35}$$

The macrostructural effective stress parameter χ^M coincides with the macrostructural degree of saturation S_r^M, i.e.

$$S_r^M = \chi^M = \begin{cases} 1 & \text{for} \quad s < s_e \\ \left(\dfrac{s_e}{s}\right)^\gamma & \text{for} \quad s \geq s_e \end{cases} \tag{36}$$

where

$$s_e = s_{en}\left(a_e + a_{scan} - a_e a_{scan}\right) \tag{37}$$

with parameter a_e and state variable a_{scan} defined as

$$a_{scan} = \frac{s - s_W}{s_D - s_W} \tag{38}$$

s_D is suction at the main drying curve and s_W at the main wetting curve corresponding to the current S_r^M. It follows that

$$s_D = \frac{s_{en}}{s_e} s \tag{39}$$

with

$$s_{en} = s_{e0}\frac{e_0^M}{e^M}\left(\frac{a+bT}{a+bT_r}\right) \tag{40}$$

a, b and T_r are parameters. The rate equation for a_{scan} reads for $s > a_e s_{en}$

$$\dot{a}_{scan} = \frac{1-r_\lambda}{s_D(1-a_e)}\dot{s} \tag{41}$$

where the ratio r_λ is defined as

$$r_\lambda = \begin{cases} 1 & \text{for} \quad s = s_D \quad \text{and} \quad \dot{s} > 0 \\ 1 & \text{for} \quad s = a_e s_D \quad \text{and} \quad \dot{s} < 0 \\ \frac{\gamma_{scan}}{\gamma} & \text{otherwise} \end{cases} \tag{42}$$

The variables $\gamma = 0.55$ and $\gamma_{scan} = \gamma/10$ denote the slopes of the main wetting-drying and scanning curves respectively. If $s \leq a_e s_{en}$, then $a_{scan} = 0$. The macrostructural effective stress rate from Eq. (34) is given by

$$\mathring{\boldsymbol{\sigma}}^M = \dot{\boldsymbol{\sigma}}^{net} + \mathbf{1}\chi^M\left[(1-r_\lambda\gamma)\dot{s} - \gamma s\frac{\dot{e}^M}{e^M} + \frac{\gamma s b\dot{T}}{a+bT}\right] \tag{43}$$

with $\dot{e}^M$ calculated using Eq. (31)b. The hypoplastic tensor $\boldsymbol{\mathcal{L}}$, which assumes transversaly isotropic material (Mašín 2014), is calculated from

$$\boldsymbol{\mathcal{L}} = \frac{1}{2}a_1\mathbf{1}\circ\mathbf{1} + a_2\mathbf{1}\otimes\mathbf{1} + a_3\left(\boldsymbol{p}\otimes\mathbf{1} + \mathbf{1}\otimes\boldsymbol{p}\right) + a_4\boldsymbol{p}\circ\mathbf{1} + a_5\boldsymbol{p}\otimes\boldsymbol{p} \tag{44}$$

The tensor $\boldsymbol{p}$ is defined as $p_{ij} = n_i n_j$, where n_i is a unit vector normal to the plane of symmetry.

$$a_1 = \alpha_E \left(1 - \nu_{pp} - 2\frac{\alpha_E}{\alpha_\nu^2}\nu_{pp}^2\right) \tag{45}$$

$$a_2 = \alpha_E \nu_{pp} \left(1 + \frac{\alpha_E}{\alpha_\nu^2}\nu_{pp}\right) \tag{46}$$

$$a_3 = \alpha_E \nu_{pp} \left(\frac{1}{\alpha_\nu} + \frac{\nu_{pp}}{\alpha_\nu} - 1 - \frac{\alpha_E}{\alpha_\nu^2}\nu_{pp}\right) \tag{47}$$

$$a_4 = \alpha_E \left(1 - \nu_{pp} - 2\frac{\alpha_E}{\alpha_\nu^2}\nu_{pp}^2\right) \frac{1 - \alpha_G}{\alpha_G} \tag{48}$$

$$a_5 = \alpha_E \left(1 - \frac{\alpha_E}{\alpha_\nu^2}\nu_{pp}^2\right) + 1 - \nu_{pp}^2 - 2\frac{\alpha_E}{\alpha_\nu}\nu_{pp}\left(1 + \nu_{pp}\right) - \frac{2\alpha_E}{\alpha_G}\left(1 - \nu_{pp} - 2\frac{\alpha_E}{\alpha_\nu^2}\nu_{pp}^2\right) \tag{49}$$

Hypoplastic barotropy factor f_s reads

$$f_s = -\frac{3\,\mathrm{tr}\,\boldsymbol{\sigma}^M}{2A_m}\left(\frac{1}{\lambda_{act}^*} + \frac{1}{\kappa^*}\right) \tag{50}$$

with λ_{act}^* calculated from (for derivation of λ_{act}^*, see Appendix B)

$$\lambda_{act}^* = \frac{\lambda^*(s,T)e^M\left(1+e^m\right) - \kappa_m\left(1+e^m\right)\left(p^M/p^m\right)\left[(1+e^M)(n_s - l_s\ln(p^M/p_r)) + f_m e^M\right]}{e^M(1+e^m) - (1+e)(n_s - l_s\ln(p^M/p_r))} \tag{51}$$

scalar A_m is calculated as

$$A_m = \nu_{pp}^2\left(\frac{4\alpha_E}{\alpha_\nu} - 2\alpha_E^2 + 2\frac{\alpha_E^2}{\alpha_\nu^2} - 1\right) + \nu_{pp}\left(\frac{4\alpha_E}{\alpha_\nu} + 2\alpha_E\right) + 2\alpha_E + 1 \tag{52}$$

The anisotropy coefficients can be calculated from

$$\alpha_E = \alpha_G^{(1/x_{GE})} \tag{53}$$

$$\alpha_\nu = \alpha_G^{(1/x_{G\nu})} \tag{54}$$

$$x_{GE} = 0.8 \tag{55}$$

$$x_{G\nu} = 1 \tag{56}$$

However, in the case of elastic isotropy assumed, α_G from (45) is equal to 1, and thus also α_E and α_ν. The hypoplastic non-linear term is governed by

$$\mathbf{N} = -\frac{\boldsymbol{\mathcal{A}} : \boldsymbol{d}}{f_s f_d^A} \tag{57}$$

with the fourth-order tensor $\boldsymbol{\mathcal{A}}$

$$\boldsymbol{\mathcal{A}} = f_s \boldsymbol{\mathcal{L}} + \frac{\boldsymbol{\sigma}^M}{\lambda^*_{act}} \otimes \mathbf{1} \tag{58}$$

and *pyknotropy* factor

$$f_d = \left(\frac{2p^M}{p_e} \right)^{\alpha_f} \tag{59}$$

The factor f_d^A controls the shape of the asymptotic state boundary surface

$$f_d^A = 2^{\alpha_f} (1 - F_m)^{\alpha_f / \omega} \tag{60}$$

The Matuoka-Nakai factor F_m reads

$$F_m = \frac{9I_3 + I_1 I_2}{I_3 + I_1 I_2} \tag{61}$$

and the scalar ω from (60) is

$$\omega = -\frac{\ln\left(\cos^2 \varphi_c\right)}{\ln 2} + a_f \left(F_m - \sin^2 \varphi_c\right) \tag{62}$$

with default value of a_f

$$a_f = 0.3 \tag{63}$$

Stress invariants I_1, I_2 and I_3 are calculated from

$$I_1 = \mathrm{tr}\boldsymbol{\sigma}^M \tag{64}$$

$$I_2 = \frac{1}{2}\left[\boldsymbol{\sigma}^M : \boldsymbol{\sigma}^M - (I_1)^2\right] \tag{65}$$

$$I_3 = \det\boldsymbol{\sigma}^M \tag{66}$$

The asymptotic strain rate direction $\boldsymbol{d}$ is given by

$$\boldsymbol{d} = \frac{\boldsymbol{d}^A}{\|\boldsymbol{d}^A\|} \tag{67}$$

with

$$\boldsymbol{d}^A = -\hat{\boldsymbol{\sigma}}^{*M} + \mathbf{1}\left[\frac{2}{3} - \frac{\cos 3\theta + 1}{4} F_m^{1/4}\right] \frac{F_m^{\xi/2} - \sin^{\xi}\varphi_c}{1 - \sin^{\xi}\varphi_c} \tag{68}$$

Lode angle function $\cos 3\theta$

$$\cos 3\theta = -\sqrt{6}\frac{\mathrm{tr}\left(\hat{\boldsymbol{\sigma}}^{*M} \cdot \hat{\boldsymbol{\sigma}}^{*M} \cdot \hat{\boldsymbol{\sigma}}^{*M}\right)}{\left[\hat{\boldsymbol{\sigma}}^{*M} : \hat{\boldsymbol{\sigma}}^{*M}\right]^{3/2}} \tag{69}$$

and

$$\xi = 1.7 + 3.9\sin^2\varphi_c \tag{70}$$

Normalised deviator stress $\hat{\boldsymbol{\sigma}}^{*M}$ reads

$$\hat{\boldsymbol{\sigma}}^{*M} = \frac{\boldsymbol{\sigma}^{*M}}{\mathrm{tr}\,\boldsymbol{\sigma}^{*M}} - \frac{\mathbf{1}}{3} \tag{71}$$

Non-linear response inside the asymptotic state boundary surface is controlled by

$$\alpha_f = \frac{\ln\left[\dfrac{\lambda^* - \kappa^*}{\lambda^* + \kappa^*}\left(\dfrac{3 + a_f^2}{a_f\sqrt{3}}\right)\right]}{\ln 2} \tag{72}$$

with

$$a_f = \frac{\sqrt{3}\,(3 - \sin\varphi_c)}{2\sqrt{2}\sin\varphi_c} \tag{73}$$

Hvorslev equivalent pressure is calculated from

$$p_e = p_r \exp\left[\frac{N(s,T) - \ln(1+e)}{\lambda(s,T)^*(s)}\right] \tag{74}$$

where $p_r = 1$ kPa is the reference stress. Values of $N(s,T)$ and $\lambda^*(s,T)$ are represented by

$$N(s,T) = N + n_s \left\langle \ln \frac{s}{s_e} \right\rangle + n_T \ln\left(\frac{T}{T_r}\right) \qquad \lambda^*(s,T) = \lambda^* + l_s \left\langle \ln \frac{s}{s_e} \right\rangle + l_T \ln\left(\frac{T}{T_r}\right) \tag{75}$$

N, λ^*, n_s, l_s n_T and l_T are model parameters. The tensorial terms $\mathbf{H}_s$ and $\mathbf{H}_T$ from Eq. (34) read

$$\mathbf{H}_s = -\frac{c_i r_\lambda \boldsymbol{\sigma}^M}{s\lambda^*_{act}} \left(n_s - l_s \ln \frac{p_e}{p_r}\right) \langle -\dot{s} \rangle \tag{76}$$

$$\mathbf{H}_T = \frac{c_i \boldsymbol{\sigma}^M}{T\lambda^*_{act}} \left(n_T - l_T \ln \frac{p_e}{p_r}\right) \langle \dot{T} \rangle \tag{77}$$

for $s > a_e s_{en}$, and $\mathbf{H}_s = \mathbf{0}$ otherwise. The factor c_i reads

$$c_i = \frac{(\lambda^*_{act} + \kappa^*)(2^{\alpha_f} - f_d) + 2\kappa^* f_d}{(\lambda^*_{act} + \kappa^*)(2^{\alpha_f} - f_d^A) + 2\kappa^* f_d^A} \tag{78}$$

The factor controlling the collapsible behaviour f_u is defined by

$$f_u = \begin{cases} \left(\frac{p^M}{p^{MA}}\right)^m & \text{for} \quad p^M \leq p^{MA} \\ \left(\frac{p^M}{p^{MA}}\right)^{100} & \text{for} \quad p^M > p^{MA} \end{cases} \tag{79}$$

where p^{MA} is the value of macrostructural effective stress corresponding to the current stress ratio at the asymptotic state boundary surface, which may be calculated as.

$$p^{MA} = \frac{p_e}{2}(f_d^A)^{1/\alpha_f} \tag{80}$$

with m being a model parameter.

The behaviour of microstructure is governed by

$$\dot{\boldsymbol{\epsilon}}^m_{nom} = \frac{\mathbf{1}}{3}\left(\alpha_s \dot{T} - \frac{\kappa_m}{p^m}\dot{p}^m\right) \tag{81}$$

$$\dot{\boldsymbol{\epsilon}}^m = (1 - f_{ul})\dot{\boldsymbol{\epsilon}}^m_{nom} \tag{82}$$

with parameter κ_m. The expression for the factor f_{ul} reads

$$f_{ul} = \begin{cases} \left(\frac{p^M}{p^{MA}}\right)^m & \text{for} \quad p^M \leq p^{MA} \quad \text{and} \quad \dot{\boldsymbol{\epsilon}}^m_{nom} > 0 \\ 1 & \text{for} \quad p^M > p^{MA} \quad \text{and} \quad \dot{\boldsymbol{\epsilon}}^m_{nom} > 0 \\ 0 & \text{for} \quad \dot{\boldsymbol{\epsilon}}^m_{nom} \leq 0 \end{cases} \tag{83}$$

$\boldsymbol{\sigma}^m$ is the microstructural effective stress given by

$$\boldsymbol{\sigma}^m = \boldsymbol{\sigma}^{net} - s = \boldsymbol{\sigma}^{tot} + u_w \tag{84}$$

The value of e^m may be initialised through

$$e^m = \exp\left[\kappa_m \ln \frac{s_r}{p^m} + \ln(1 + e^m_{r0}) + \alpha_s \left(T - T_r\right)\right] - 1 \tag{85}$$

with parameters e^m_{r0}, s_r and T_r.

Finally, the double-structure coupling function f_m reads

$$f_m = \begin{cases} 1 - (r_{em})^m & \text{for} \quad \dot{p}^m \leq 0 \\ \langle \frac{c_{sh} s}{s_e} \rangle & \text{for} \quad \dot{p}^m > 0 \end{cases} \tag{86}$$

while $f_m = 1$ if Eq. (86) leads to $f_m > 1$. r_{em} is relative void ratio

$$r_{em} = \frac{e - e_d}{e_i - e_d} \tag{87}$$

with

$$e_i = \exp\left[N(s,T) - \lambda^*(s,T)\ln p^M\right] - 1 \tag{88}$$

and

$$e_d = e_m \tag{89}$$

APPENDIX B - DERIVATION OF THE SLOPE OF NORMAL COMPRESSION LINE

In this appendix, derivation of λ^*_{act} is described. Time derivative of the normal compression line formulation (88), accompanied with (75), (37) and (40) and acknowledging that the hypoplastic model predicts macrostructural strains $\mathrm{tr}\,\dot{\boldsymbol{\epsilon}}^M$ yields

$$\mathrm{tr}\,\dot{\boldsymbol{\epsilon}}^M = -\lambda^*(s,T)\frac{\dot{p}^M}{p^M} + \left(n_s - l_s \ln\frac{p^M}{p_r}\right)\frac{\dot{e}^M}{e^M} \tag{90}$$

Further, it follows from (32) that

$$\dot{e} = \dot{e}^M\left(1+e^m\right) + \dot{e}^m\left(1+e^M\right) \tag{91}$$

Eqs. (22) and (31)c imply (note that f_{ul} is zero for microstructural shrinkage)

$$\frac{\dot{e}^m}{1+e^m} = -\kappa_m\frac{\dot{p}^m}{p^m} \tag{92}$$

The expression for λ^*_{act} is derived for mechanical loading at constant suction, for which $\dot{p}^M \approx \dot{p}^m$ (change of S_r^M during loading has been neglected). Under this assumption, combination of (92) with (91) yields

$$\dot{e}^M = \frac{\dot{e}}{1+e^m} + \kappa_m\frac{\dot{p}^M}{p^m}\left(1+e^M\right) \tag{93}$$

It also follows from (30) and (31) together with the assumption $\dot{p}^M \approx \dot{p}^m$ that

$$\frac{\dot{e}}{1+e} = \mathrm{tr}\left(\dot{\boldsymbol{\epsilon}}^M + f_m\dot{\boldsymbol{\epsilon}}^m\right) = \mathrm{tr}\,\dot{\boldsymbol{\epsilon}}^M - f_m\kappa_m\frac{\dot{p}^M}{p^m} \tag{94}$$

Now, we can combine (90), (93) and (94), which after rearrangement yields

$$\frac{\dot{e}}{1+e}\left(1-\frac{(1+e)[n_s-l_s\ln(p^M/p_r)]}{e^M(1+e^m)}\right)= \\ \frac{\dot{p}^M}{p^M}\left(-\lambda^*(s,T)+\frac{p^M}{p^m}\left[n_s-l_s\ln(p^M/p_r)\right]\frac{\kappa_m(1+e^M)}{e^M}+\kappa^m f_m\frac{p^M}{p^m}\right) \tag{95}$$

Eq. (95) can finally be compared with

$$\frac{\dot{e}}{1+e}=-\lambda^*_{act}\frac{\dot{p}^M}{p^M} \tag{96}$$

leading to

$$\lambda^*_{act}=\frac{\lambda^*(s,T)e^M\left(1+e^m\right)-\kappa_m\left(1+e^m\right)\left(p^M/p^m\right)\left[(1+e^M)(n_s-l_s\ln(p^M/p_r))+f_m e^M\right]}{e^M(1+e^m)-(1+e)(n_s-l_s\ln(p^M/p_r))} \tag{97}$$

List of Tables

Table 1. ***Summary of model parameters.***

Parameter	Description
φ_c	Critical state friction angle of macrostructure in a standard soil-mechanics meaning.
λ^*	Slope of the isotropic normal compression line in the $\ln(p^M/p_r)$ vs. $\ln(1+e)$ space.
κ^*	Controls macrostructural volume strain in p^M unloading.
N	Position of the isotropic normal compression line in the $\ln(p^M/p_r)$ vs. $\ln(1+e)$ space.
ν	Parameter controlling stiffness in shear.
n_s	Controls the dependency of position of the isotropic normal compression line on suction.
l_s	Controls the dependency of slope of the isotropic normal compression line on suction.
n_T	Controls the dependency of position of the isotropic normal compression line on temperature.
l_T	Controls the dependency of slope of the isotropic normal compression line on temperature.
m	This parameter is present twice within the model formulation. First of all, it controls the factor f_u and thus the dependency of the wetting- and heating-induced compaction on the distance from the state boundary surface (the higher the value of m, the closer the state needs to be to the state boundary surface for the compaction to become significant). Second, the parameter m controls the double-structure coupling function and it thus affects the response to wetting-drying and heating-cooling cycles (see Mašín (2013b)).
α_s	Controls the dependency of microstructural volume strains on temperature.
κ_m	Controls the dependency of microstructural volume strains on p^m.
e^m_{r0}	Represents reference microstructural void ratio for the reference temperature T_r, reference suction s_r and zero total stress.
c_{sh}	Parameter controlling the value of f_m for compression.
s_{e0}	Air-entry value of suction for reference macrostructural void ratio e^M_0.
a	Controls the dependency of the macrostructural air-entry value of suction on temperature.
b	Controls the dependency of the macrostructural air-entry value of suction on temperature.
a_e	Ratio of the air-entry and air-expulsion values of suction of the water retention model for macrostructure.
s_r	Reference suction for e^m calculation.
e^M_0	Reference macrostructural void ratio for calculation of the air-entry value of suction of macrostructure.
T_r	Reference temperature.

Table 2. ***Parameters of the proposed model for MX80 bentonite.***

parameter	value
φ_c	25°
λ^*	0.081
κ^*	0.01
N	1.48
ν	0.25
n_s	0.005
l_s	0.0048
n_T	-0.07
l_T	0
m	35
α_s	0.00015 K^{-1}
κ_m	0.18
e_{r0}^m	0.12
c_{sh}	0.002
s_{e0}	200 kPa
a	0.118
b	-0.000154
a_e	0.75
s_r	140 MPa
e_0^M	0.5
T_r	294 K

List of Figures

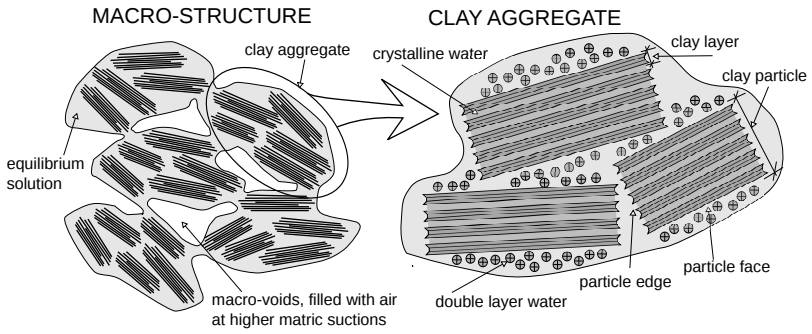

Figure 1. A conceptual sketch of two levels of structure considered in double-structure models.

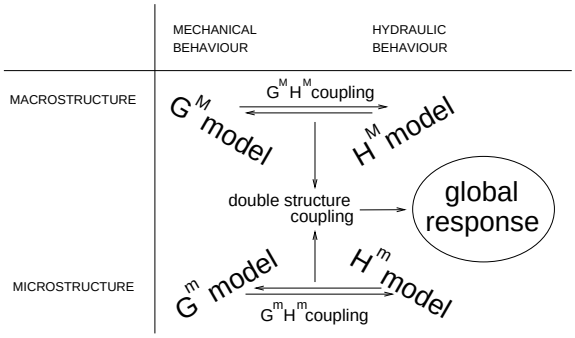

Figure 2. Schematic representation of the modelling approach adopted in this paper.

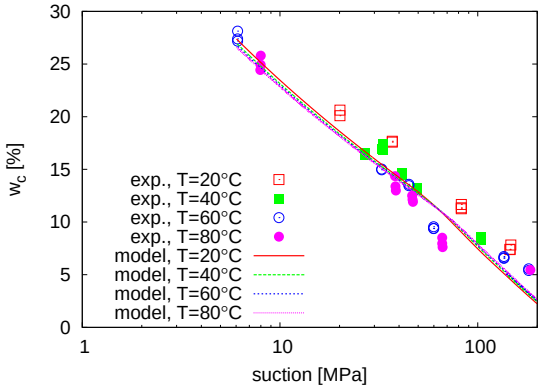

Figure 3. Water retention curves at different temperatures: experimental data (Tang and Cui 2007) compared with model predictions.

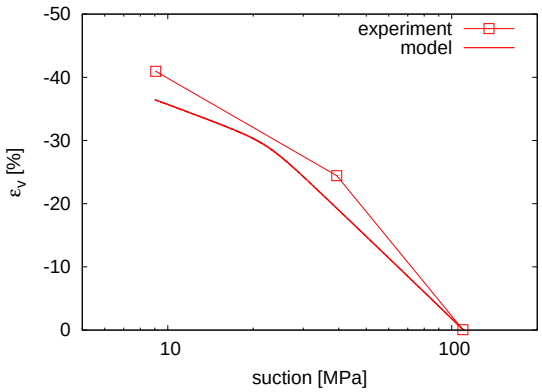

Figure 4. Swelling strains developed during wetting of the samples later tested in suction- and temperature-controlled isotropic cell. Experimental data (Tang et al. 2008) compared with model predictions.

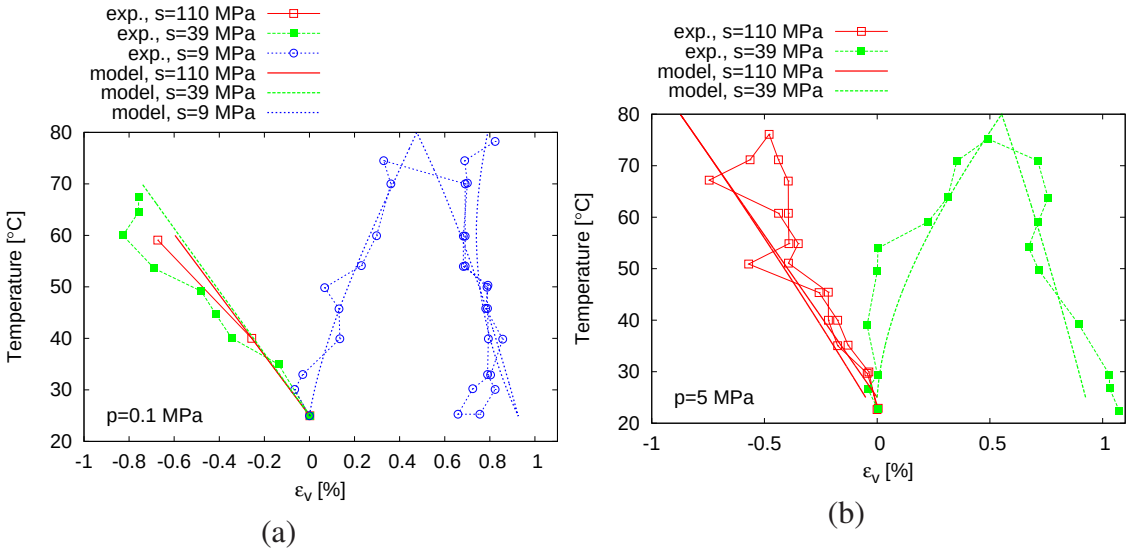

Figure 5. Volume change due to heating and cooling at total isotropic stresses of 0.1 MPa (a) and 5 MPa (b). Experimental data (Tang et al. 2008) compared with model predictions.

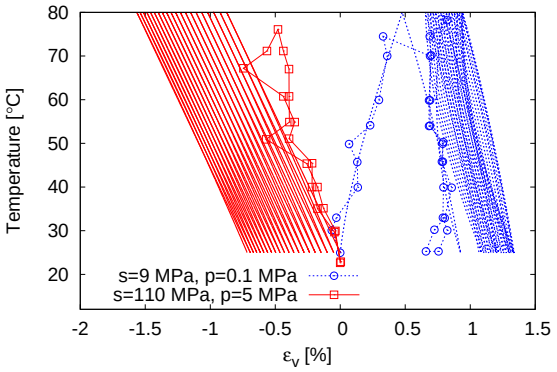

Figure 6. Volume change due to heating and cooling cycles. Selected simulations from Fig. 5 continued for 20 cycles.

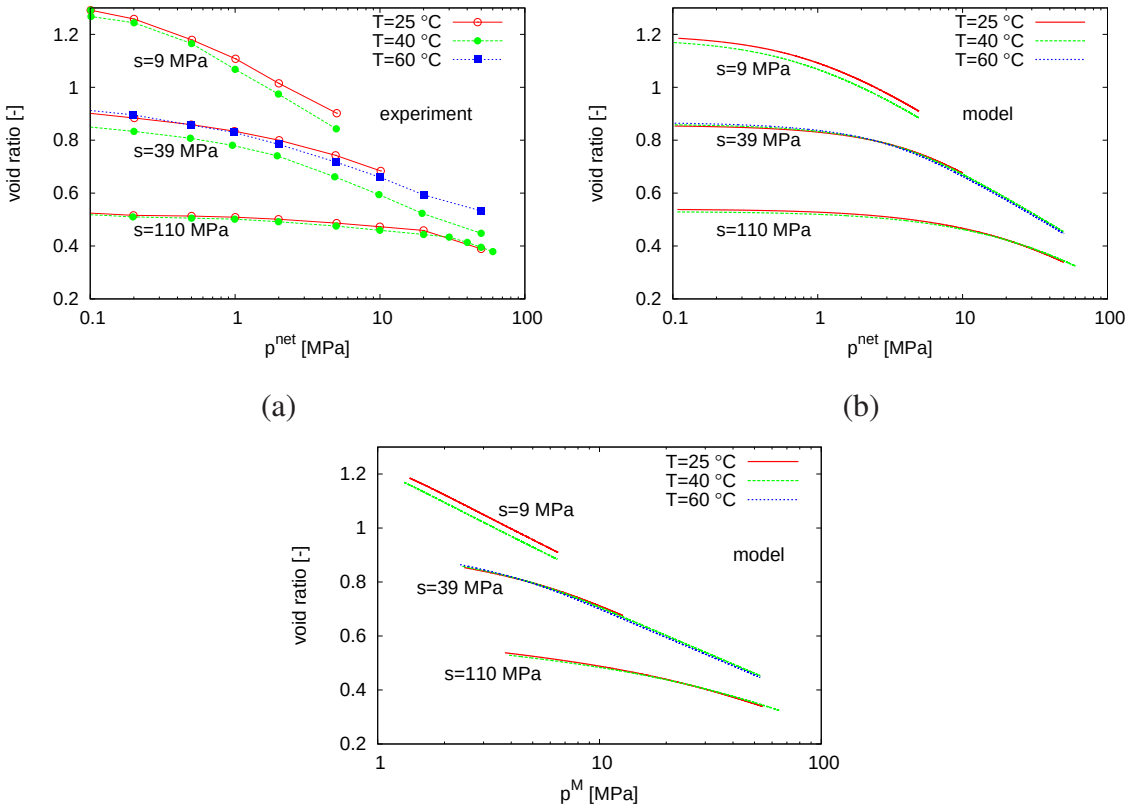

Figure 7. Isotropic compression tests at various suctions and temperatures. (a) experimental data from Tang et al. (2008), (b) predictions in terms of net stress, (c) predictions in terms of macrostructural effective stress.